Journal Name

Dynamic Article Links ►

Cite this: DOI: 10.1039/c0xx00000x

www.rsc.org/xxxxxx

ARTICLE TYPE

Catalytic N-oxidation of tertiary amines on RuO_2NPs anchored graphene nanoplatelets

Mayakrishnan Gopiraman,[a] Hyunsik Bang,[a] Sundaram Ganesh Babu,[a,b] Kai Wei,*[a,c] Ramasamy Karvembu*[d] and Ick Soo Kim *[a]

Received (in XXX, XXX) Xth XXXXXXXXX 20XX, Accepted Xth XXXXXXXXX 20XX

DOI: 10.1039/b000000x

Ultrafine ruthenium oxide nanoparticles (RuO_2NPs) of an average diameter of 1.3 nm were anchored on graphene nanoplatelets (GNPs) using $Ru(acac)_3$ precursor by a very simple dry synthesis method. The resultant material (GNPs-RuO_2NPs) was used as a heterogeneous catalyst for the N-oxidation of tertiary amines for the first time. The transmission electron microscopic (TEM) images of the GNPs-RuO_2NPs showed an excellent attachment of RuO_2NPs on GNPs. The loading of Ru in GNPs-RuO_2NPs was 2.68 wt%, as confirmed by scanning electron microscope-energy dispersive spectroscopy (SEM-EDS). X-ray photoelectron spectrum (XPS) and X-ray diffraction pattern (XRD) of GNPs-RuO_2NPs revealed that the chemical state of Ru on GNPs was +4. After the optimization of reaction conditions for N-oxidation of triethylamine, the scope of the reaction was extended with a various aliphatic, alicyclic and aromatic tertiary amines. The GNPs-RuO_2NPs showed an excellent catalytic activity in terms of yields even at a very low amount of Ru catalyst (0.13 mol%). The GNPs-RuO_2NPs was heterogeneous in nature, chemically as well as physically very stable and reused for up to 5 times.

Introduction

Aliphatic and aromatic *tert*-amine oxides (amine N-oxides) are essential and key components in the formulation of several cosmetic products as well as in biomedical applications.[1,2] Particularly, N-oxides of aromatic amines are extensively used as protecting groups, auxiliary agents, and oxidants in various organic reactions.[3,4] They often used as potential cytoxymes for the treatment of solid tumors and also as ligands for the preparation of useful transition metal complexes.[5,6] As a catalyst, especially in epoxidation reactions, amine N-oxides displayed a wide range of advantages in chemical industries.[7] Notably, enantiopure chiral N-oxides, found to play a substantial role as a Lewis base catalyst in asymmetric transformation.[8] However, traditionally, these amine N-oxides are prepared *via* a noncatalytic oxidation processes using α-azo hydroperoxides,[9] activated H_2O_2,[10] Caro's acid (H_2SO_5),[11] dioxiranes,[12] peracids,[13] and magnesium monophthalate.[14] These reagents are not only expensive and toxic, but also produce a large amount of effluents during the reaction, which often lead to the environmental problem of waste disposal. To prevent this issue, catalytic oxidation processes using environmental friendly oxidants such as air, O_2 and H_2O_2 have been developed. Silica supported vanadium,[15] biomimetic methyltrioxorhenium(VII) or manganese porphyrin,[16] titanium molecular sieves [TiMCM-41 and TiZSM-5(30)],[17] tungsten-based polyperoxometalates,[18] tungstate-exchanged Mg/Al-layered double hydroxide acid (LDH-WO_4),[19] vanadium-silicate molecular sieve,[20] and titanium silicalite (TS-1) materials[21] have been proposed as heterogeneous catalysts for the oxidation of tertiary amines to their corresponding N-oxides using H_2O_2 as an oxidant. Owing to the recyclability and easy separation from the reaction mixture, metal nanoparticles (MNPs), particularly supported MNPs, played a tremendous role in heterogeneous catalysis. There are very few MNPs supported on carbon materials, particularly carbon black, employed as a catalyst for this oxidation reaction. Unfortunately, most of them have shown less activity in N-oxidation of tertiary amines.[22] Pina *et al*., investigated the activity of gold-based mono- and bi-metallic catalysts in the oxidation of tertiary amines to afford the corresponding N-oxides.[23] They found that Au/C catalyst showed an excellent catalytic activity for the oxidation of tertiary amines to the corresponding N-oxides; however, other catalysts namely Rh/C, Pt/C, AuRh/C and AuPt/C are less effective and often require alkali as a promoter to improve the activity of the catalysts.[23] In addition to the high cost of the Au, Pt and Rh catalysts, they often require higher stoichiometric amount of catalyst for the N-oxidation reaction. Therefore, developing an efficient and recyclable catalytic system with the use of lower amount of catalyst remains a challenging task.

Among the noble metal catalysts, ruthenium has shown high catalytic activity mainly in oxidation reactions.[24-27] Very recently, due to the astounding properties of graphene such as high surface area and chemical inertness, it has been receiving a great deal of attention as a support for active metal catalysts including RuNPs in heterogeneous catalysis.[28] According to Krasheninnikov *et al*., the inert graphene can be transformed into a very active catalyst through the interactions between the active metal clusters and carbon vacancies.[29] In our previous work on the aerial oxidation

of alcohols, we found that RuNPs decorated graphene nanosheets (GNSs) catalyst is efficient, reusable, chemically as well as physically very stable and the catalytic system required a low amount of Ru (0.036 mol%).[30] Similarly, GNPs-RuO_2NRs composite was prepared by a simple dry synthesis method and was used as an efficient nanocatalyst for the transfer hydrogenation of carbonyl compounds.[31] Inspired by these results, we have used GNPs-RuO_2NRs composite as catalyst in N-oxidation reactions too. However, the GNPs-RuO_2NRs showed less catalytic activity in the N-oxidation reactions. Hence, herein, we report the simple preparation of graphene nanoplatelets (GNPs) supported ultrafine RuO_2NPs catalyst and its activity towards N-oxidation of tertiary amines.

Experimental

Materials and characterization

GNPs (purity: >99 wt%, surface area: >750 m^2/g, average thickness: 3 nm, layers: <5, diameter: 1-2 μm) were purchased from Cheap Tubes Inc., VT, US. Ru(acac)$_3$ (97%) and all other chemicals were purchased form Aldrich and used as received.

The morphology of the prepared nanocatalysts (GNPs-RuO_2NPs) was investigated by TEM (JEM-2100 JEOL Japan) with accelerating voltage of 200 kV. The weight percentage and homogeneous decoration of RuO_2NPs on GNPs were confirmed by SEM-EDS (Hitachi 3000H). The same field of view was then scanned using an EDS spectrometer to acquire a set of X-ray maps at 1 ms point acquisition for approximately one million counts. The interaction of RuO_2NPs with GNPs was examined by Raman spectrometer (Hololab 5000, Kaiser Optical Systems Inc., USA) using argon laser at 532 nm with a Kaiser holographic edge filter. Wide angle XRD experiments were performed at room temperature using a Rotaflex RTP300 (Rigaku.Co., Japan) instrument at 50 kV and 200 mA. Nickel-filtered Cu Kα radiation ($5^o > 2\theta < 80^o$) was used for the XRD measurements. To confirm the chemical state of Ru, XPS spectrum was recorded in Kratos Axis-Ultra DLD instrument. The samples were irradiated under Mg Kα ray source before XPS analysis. NMR spectra were recorded on a 400 MHz Bruker spectrometer in $CDCl_3$ using tetramethylsilane as a standard. FT-IR spectra were recorded using a Horiba FT-720 IR spectrophotometer.

Dry synthesis of nanocatalyst (GNPs-RuO_2NPs)

In order to introduce oxygen functional groups on GNPs, initially, it was subjected to chemical treatment according to the literature procedure.[32] In a typical procedure, the GNPs (1.0 g) was chemically treated with a 3:1 ratio mixture of concentrated H_2SO_4 and HNO_3. Subsequently, the resulting mixture was sonicated at 40^oC for 3 h in an ultrasonic bath. After cooling to room temperature, the mixture was diluted with 750 mL of double distilled water and then vacuum-filtered. The resultant solid (*f*-GNPs) was repeatedly washed with double distilled water until the pH reached neutral and then vacuum dried at 60^oC. After that, 50 mg of Ru(acac)$_3$ was added into 500 mg of *f*-GNPs and mixed well by a mortar and pestle under ambient condition. The homogeneous mixture of *f*-GNPs and Ru(acac)$_3$ was obtained within 10-15 minutes. Finally, the impregnated Ru(acac)$_3$ was thermally decomposed into RuO_2NPs by calcinating at 350^oC for 6 h under nitrogen atmosphere. Fig. 1 shows a schematic illustration of the procedure for preparation of the GNPs-RuO_2NPs.

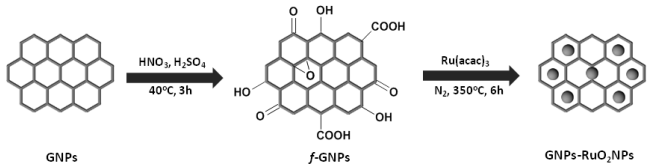

Fig. 1 Schematic diagram of the preparation of GNPs-RuO_2NPs.

Oxidation of tertiary amines

10 mg of GNPs-RuO_2NPs (0.13 mol%) was stirred with 3 mL of CH_3CN taken in a round-bottomed flask equipped with a condenser and a stirring bar. To the above mixture, substrate (2 mmol) was added followed by a slow dropwise addition of 30% H_2O_2 (5 mmol). Then the solution mixture was heated at 80^oC under atmospheric pressure of air. The completion of the N-oxidation reaction was monitored by TLC. Once the reaction completed, the nanocatalyst was separated out from the reaction mixture by simple centrifugation, washed well with diethyl ether followed by drying in an oven at 80^oC for 3 h and was reused for the subsequent N-oxidation of tertiary amines. In other hand, the centrifugate was dried over anhydrous $MgSO_4$ to afford the product which was purified by passing through a column of silica gel using dichloromethane-MeOH (90:10) as an eluent. The products (amine N-oxides) were identified by NMR and FT-IR spectral data. Some of the products (Table 1, entries 4, 5, 8, 12, 13, 15 and 17) are known compounds and were identified by the comparison of their spectral features with the respective reported data.

Triethylamine N-oxide (Table 1, entry 1): Yellow liquid; ^{1}H-NMR (400 MHz, DMSO-d_6): δ 1.10-1.14 (t, 9H), 2.99-3.05 (m, 6H); ^{13}C-NMR (400 MHz, DMSO-d_6): δ 8.4, 58.8; FT-IR (cm^{-1}): 3145, 1685, 1392, 1150, 825.

N,N-Dimethyl aniline N-oxide (Table 1, entry 2): Yellow solid; ^{1}H-NMR (400 MHz, DMSO-d_6): δ 2.65 (s, 6H), 6.62-6.64 (m, 1H), 6.71-7.73 (m, 3H), 7.15-7.19 (m, 2H); ^{13}C-NMR (400 MHz, DMSO-d_6): δ 40.5, 111.9, 112.7, 116.4, 129.2, 150.8; FT-IR (cm^{-1}): 2933, 1591, 1500, 1341, 1223, 1190, 1164, 1063, 1030, 1000, 943, 750, 689.

N,N-Dimethyl-p-toluidine N-oxide (Table 1, entry 3): Yellow solid; ^{1}H-NMR (400 MHz, DMSO-d_6): δ 2.25 (s, 3H), 2.89 (s, 6H), 6.68-6.70 (d, J = 8 Hz, 2H), 7.04-7.06 (d, J = 8 Hz, 2H); ^{13}C-NMR (400 MHz, DMSO-d_6): δ 20.3, 113.1, 125.0, 129.7, 148.1; FT-IR (cm^{-1}): 3389, 2932, 2879, 2868, 1676, 1623, 1523, 1330, 1154, 1050, 952, 799, 713, 687.

N,N-Dimethyl-o-toluidine N-oxide (Table 1, entry 4): Yellow solid; ^{1}H-NMR (400 MHz, DMSO-d_6): δ 2.25 (s, 3H), 2.61 (s, 6H), 6.91-7.14 (m, 4H); FT-IR (cm^{-1}): 2967, 1569, 1493, 1450, 1310, 1185, 1155, 1117, 1050, 950, 760, 723.

N,N-Dimethyl-m-toluidine N-oxide (Table 1, entry 5): Yellow solid; ^{1}H-NMR (400 MHz, DMSO-d_6): δ 2.24 (s, 3H), 2.86 (s, 6H), 6.46-6.48 (m, 1H), 6.48-6.51 (m, 1H), 6.53 (s, 1H), 7.03-

7.07 (m, 1H); FT-IR (cm^{-1}): 2935, 2825, 1679, 1626, 1518, 1339, 1157, 1059, 960, 810, 773, 689.

4-Bromopyridine N-oxide (Table 1, entry 8): Pale brown solid; ^{1}H-NMR (400 Hz, DMSO-d_6): δ 7.85-7.86 (d, *J* = 4.0 Hz, 2H), 8.73-8.74 (d, *J* = 4.0 Hz, 2H); FT-IR (cm^{-1}): 3023, 2531, 1619, 1475, 1360, 1342, 1102, 1084, 794, 725.

2-Bromopyridine N-oxide (Table 1, entry 9): Pale brownish yellow liquid; ^{1}H-NMR (400 Hz, DMSO-d_6): δ 7.44-7.47 (m, 1H), 7.64-7.66 (d, *J* = 8.0 Hz, 1H), δ 7.75-7.79 (m, 1H), 8.39-8.41 (m, 1H); ^{13}C-NMR (400 MHz, DMSO-d_6): δ 123.8, 128.6, 140.0, 141.8, 150.9; FT-IR (cm^{-1}): 3050, 1560-1580, 1451, 1410, 1100-1080, 991, 758, 699.

Quinoline N-oxide (Table 1, entry 11): Colorless solid; ^{1}H-NMR (400 MHz, DMSO-d_6): δ 7.51-8.05 (m, 5H), 8.35-8.37 (d, *J* = 8 Hz, 1H), 8.91-8.92 (m, 1H); ^{13}C-NMR (400 MHz, DMSO-d_6): δ 121.8, 126.9, 128.4, 129.2, 129.8, 130.0, 136.3, 148.0, 150.6; FT-IR (cm^{-1}): 3562, 3029, 1492, 1428, 1388, 1298, 1265, 1219, 1204, 1176, 1136, 1086, 1052, 1010, 877, 829, 763,732.

Quinoxaline N-dioxide (Table 1, entry 12): Yellow solid; ^{1}H-NMR (400 MHz, DMSO-d_6): δ 7.74-7.87 (m, 2H), 8.12 (m, 2H), 8.86 (s, 2H); FT-IR (cm^{-1}): 3411, 3046, 1675, 1485, 1372, 1202, 1126, 1020, 950, 863, 750.

2,2'-Bipyridyl N-dioxide (Table 1, entry 13): Gray solid; ^{1}H-NMR (400 Hz, DMSO-d_6): δ 7.45-7.47 (m, 2H), 7.95-7.97 (m, 2H), 8.38-8.40 (d, *J* = 8.0 Hz, 2H), 8.69-8.70 (d, *J* = 4.0 Hz, 2H); FT-IR (cm^{-1}): 2900, 2825, 2201, 1622, 1520-1530, 1503, 1350-1370, 1225, 1100, 1060, 980, 789, 657.

4-(Dimethylamino)pyridine N-dioxide (Table 1, entry 17): Colorless solid; ^{1}H-NMR (400 Hz, DMSO-d_6): δ 2.94 (s, 6H), 6.57-6.59 (d, *J* = 8.0 Hz, 2H), 8.09-8.11 (d, *J* = 8.0 Hz, 2H); FT-IR (cm^{-1}): 2901, 2832, 1520-1532, 1432, 1350-1374, 1225, 1108, 1064, 985, 806, 745, 655.

1-Phenylpiperazine N-dioxide (Table 1, entry 18): Yellow liquid; ^{1}H-NMR (400 Hz, DMSO-d_6): δ 1.8 (s, 1H), 3.01-3.03 (m, 2H), 3.12-3.15 (m, 2H), 6.83-6.94 (m, 3H), 7.24-7.28 (m, 2H); FT-IR (cm^{-1}): 2900, 2825, 1594, 1500-1530, 1434, 1350-1374, 1225, 1114, 1064, 980, 799.

Results and discussion

Characterization of GNPs-RuO_2NPs

To investigate the morphology of GNPs-RuO_2NPs, TEM images were taken for pure GNPs and GNPs-RuO_2NPs [Fig. 2(i-v)]. The TEM image of pure GNPs confirmed the presence of irregular ultra thin sheets of size ranging from 0.5 to 2 µm. GNPs also has multi layers with an average thickness of about 7-9 nm. As can be seen from the TEM images of GNPs-RuO_2NPs, an ultra-fine RuO_2NPs were homogeneously dispersed on the surface of GNPs. High magnified TEM images of GNPs-RuO_2NPs showed good adhesion of RuO_2NPs on anchoring sites of GNPs with very narrow particle size distribution. The histogram of RuO_2NPs reveals that the RuO_2NPs have a very narrow size distribution ranging from 0.5 to 3.0 nm with a peak centered at *ca.* 1.3 nm [Fig. 2(vi)]. It is worth to mention that there was no free RuO_2NPs were observed in the background of the TEM images, which confirmed the complete utilization of the RuO_2NPs by the GNPs. In addition, the surface area per unit mass (*S*) of RuO_2NPs

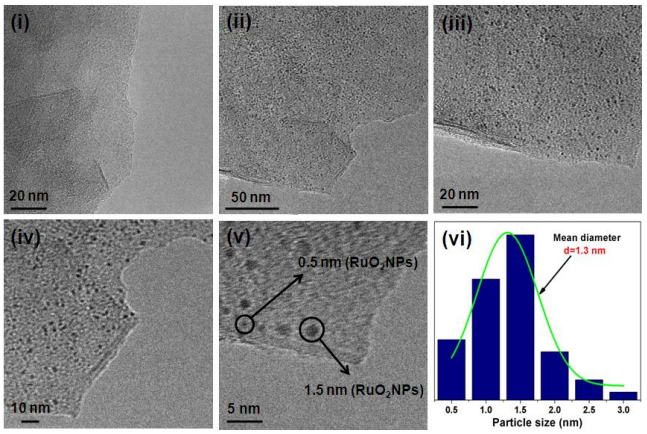

Fig. 2 TEM images of (i) pure GNPs and (ii, iii, iv and v) GNPs-RuO_2NPs, and (vi) the particle size distribution of RuO_2NPs.

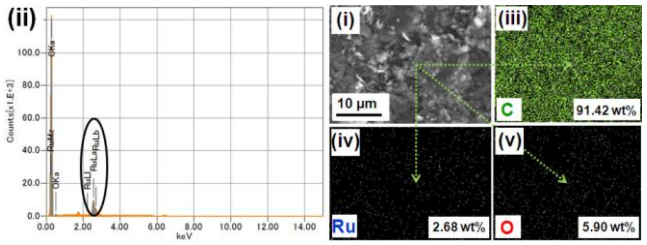

Fig. 3 (i) SEM images and (ii) corresponding EDS spectrum of GNPs-RuO_2NPs, and EDS mapping of (iii) C, (iv) Ru and (v) O.

was calculated by using the equation,[30] $S = 6000/(\rho \times d)$ where *d* is the mean diameter of RuO_2NPs (1.3 nm), and ρ is the density of RuO_2 (6.97 gcm^{-3}) and it was found to be 1119.40 m^2g^{-1}. Fig. 3 shows the SEM-EDS and corresponding elemental mapping images of GNPs-RuO_2NPs. The weight percentage of Ru in GNPs-RuO_2NPs was 2.68 as determined by EDS analysis [Fig. 3(ii)]. As expected, EDS mapping analysis confirms the homogeneous distribution of RuO_2NPs in GNPs-RuO_2NPs. The credibility of the proposed method can be understood from the purity of GNPs-RuO_2NPs that contains only carbon, ruthenium and oxygen elements as confirmed by EDS analysis.

XPS spectra were recorded for *f*-GNPs and GNPs-RuO_2NPs in order to confirm the functionalization of GNPs and the chemical state of Ru in GNPs-RuO_2NPs; the results are shown in Fig. 4(i and ii) and Fig. 5(i and ii). As expected, both *f*-GNPs and

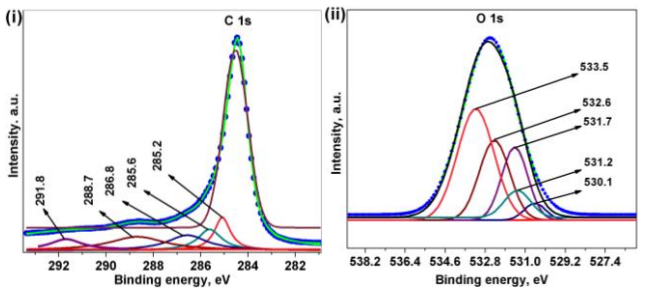

Fig. 4 XPS spectrum of *f*-GNPs; magnified (i) C 1s and (ii) O 1s peaks.

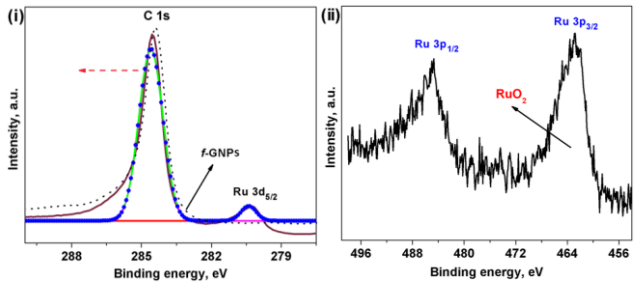

Fig. 5 XPS spectrum of GNPs-RuO_2NPs; magnified (i) C 1s and (ii) Ru 3p peaks.

GNPs-RuO_2NPs showed a C 1s peak and O 1s peak at 284.5 and 532.5 eV respectively [Fig. 4(i and ii) and Fig. 5(i)]. The binding energy of C–C, C–O–C, C=O and –COOH groups is assigned at 285.2, 285.6, 286.8 and 288.7 eV respectively.[33] Deconvolution of the O 1s spectrum of *f*-GNPs [Fig. 5(ii)] resulted in five peaks located at 530.1, 531.2, 531.7, 532.6 and 533.5 eV, which were assigned to the C=O, –COOH, C–OH, –C–O–C– and H_2O respectively.[34] According to Gil *et al*.,[35] oxygen functional groups on graphene act as effective nucleation centers for MNPs, which assist homogeneous decoration as well as better adhesion of MNPs on graphene. Likewise in the present case, the homogeneous as well as better adhesion of RuO_2NPs on GNPs [Fig. 2(i-v)] are due to the presence of oxygen functional groups on GNPs. Particularly, –COOH group assists good adhesion of RuO_2NPs on GNPs by replacing the proton of –COOH.[36] The XPS spectrum of GNPs-RuO_2NPs [Fig. 5(i and ii)] showed binding energy (BE) of Ru $3p_{3/2}$ at 462.5 eV, Ru $3p_{1/2}$ at 485.0 eV and Ru $3d_{5/2}$ at 280.8 eV, which correspond to the photoemission from RuO_2.[37] The overlapping of the C 1s and the Ru $3d_{3/2}$ peaks at ~285 eV makes it difficult to assign BE of Ru $3d_{3/2}$. The chemical state of Ru was also confirmed by XRD [Fig. 6(i)]. The diffraction peaks at 26.5, 44.2 and 54.8°, corresponding to the (002), (100), and (004) crystal planes of graphite respectively, attributed to the hexagonal graphite structures of GNPs.[38] The very weak XRD peaks at 27.5, 34.9, 39.9 and 57.5° correspond to the typical crystal faces (110), (101), (200) and (220) of RuO_2 (JCPDS 21-1172) respectively, confirmed the nano-crystalline nature of RuO_2.[38]

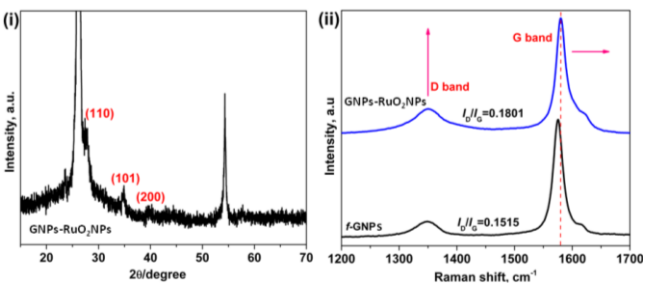

Fig. 6 (i) XRD pattern of GNPs-RuO_2NPs and (ii) Raman spectra of *f*-GNPs and GNPs-RuO_2NPs.

The Raman spectroscopy is a precise and quick analysis method to investigate the nature of interaction between various MNPs and graphene. Therefore, Raman spectrum was recorded for GNPs-RuO_2NPs under 514.5 nm excitation over the Raman shift interval of 250-4000 cm^{-1} [Fig. 6(ii)]. As expected, both *f*-GNPs and GNPs-RuO_2NPs exhibited two main Raman features, corresponding to the well-defined D-band line at ~1345 cm^{-1} and G-band line at ~1570 cm^{-1}. The G-band line is originated from in-plane vibration of sp^2 carbon atoms, which represents the relative degree of graphitization.[39] The D-band line is related to the amount of disorder which arises only in the presence of defects, indicating the presence of sp^3 carbon atoms or defect sites in GNPs.[38] Since the ratio of D and G band (*ID*/*IG*) intensities is often used as a diagnostic tool to evaluate the defects concentration in graphene, it was calculated for *f*-GNPs and GNPs-RuO_2NPs. It is noteworthy that the *ID*/*IG* (0.1801) ratio of GNPs-RuO_2NPs was higher than that of *f*-GNPs (0.1515), which confirmed that the RuO_2NPs are attached on the surface of GNPs with good adhesion. In the XPS spectrum [Fig. 5(i)], a significant positive shift in C 1s peak was observed for GNPs-RuO_2NPs when compared to that of the *f*-GNPs; this too confirms there has been a very strong interaction between GNPs and RuO_2NPs.[39,40]

Optimization of reaction condition for the N-oxidation of triethylamine

To find out the most effective reaction condition for the N–oxidation of tertiary amines, in a preliminary study, we used triethylamine as a substrate and varied the solvent, amount of catalyst, time, amount of oxidant and temperature [Fig. 7(i-iv)]. In solvent optimization, various solvents such as toluene, $CHCl_3$ and CH_3OH were used but they were less effective compared to CH_3CN [Fig. 7(i)]. As expected, only a very less amount of triethylamine N-oxide was obtained in the absence of the catalyst. 10 mg of the catalyst (0.13 mol% of Ru) was enough for the N-oxidation of triethylamine; this is the lowest amount of Ru catalyst reported for the N-oxidation of tertiary amines till to date. In temperature optimization, a maximum yield of 98% was obtained when the reaction was stirred at 80°C [Fig. 7(ii)].

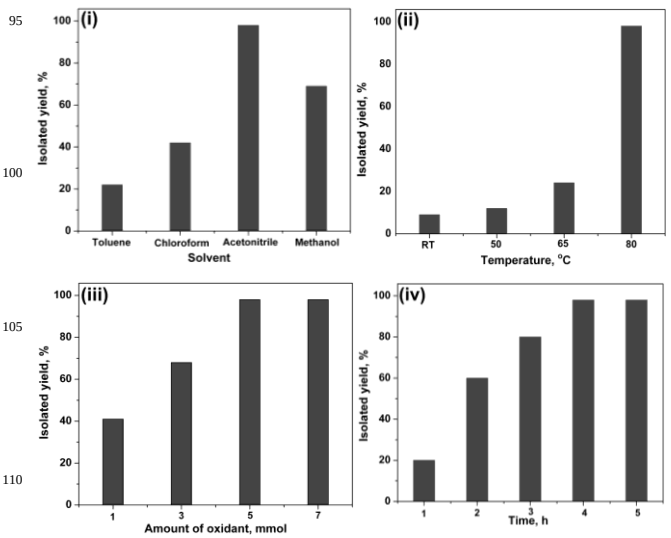

Fig. 7 Effect of (i) solvent, (ii) temperature, (iii) amount of oxidant and (iv) time on the N-oxidation of triethylamine.

Amount of oxidant played a significant role in the N-oxidation process. It was found that 5 mmol of H_2O_2 was an optimum amount of oxidant [Fig. 7(iii)]. An excellent yield of 98% was obtained when the reaction mixture was stirred for 4 h [Fig. 7(iv)]. The optimized reaction condition was opted to extend the scope of the N–oxidation of tertiary amines.

Extension of scope

Table 1 shows a variety of tertiary amines which were oxidized to their corresponding N-oxides in good to excellent yields. The yield of products was moderately affected by the substituent in the substrate. Aliphatic tertiary amine, triethylamine, was oxidized to triethylamine N-oxide in excellent yield of 98% (Table 1, entry 1) whereas Pt/C gave a lower yield of 66%.[23] However, under the same reaction condition, the GNPs-RuO_2NRs composite[31] gave the product (triethylamine N-oxide) in a moderate yield of 72%. The better activity of the present catalyst is due to the ultrafine nature of the RuO_2NPs compared to the RuO_2NRs. Similarly, N,N-dimethyl aniline (DMA) gave the corresponding N-oxide in a better yield of 98% (Table 1, entry 2) in comparison to the Ti–MCM-41 system.[41] It was found that the DMA containing electron donating group such as methyl (–CH_3), reacted faster whereas DMA with electron withdrawing group (–CN or –COOH) required extended reaction time to afford even the less amount of corresponding N-oxide, which may be due to the mesomeric effect (Table 1, entries 3-7). The present catalytic system showed a better yield for these substrates in comparison to the Pd catalytic system.[42]

Very recently, pyridine N-oxides have been recognized as a new class of anti-HIV compounds.[43] Therefore, the present catalytic system was adopted to prepare some pyridine N-oxide derivatives. Interestingly, pyridine containing electron withdrawing group such as -Br at *para* position gave the corresponding N-oxide in excellent yield of 93% (Table 1, entry 8) whereas $H_{14}P_5Mo$ system afforded only a trace amount of the same product.[43] Alike, 2-bromopyridine was also oxidized to the corresponding N-oxide in a good yield of 87% (Table 1, entry 9). In the oxidation of 6-(dimethylamino)fulvene, the present catalytic system gave an excellent yield of 92% after stirring for 6 h (Table 1, entry 10). For the transformation of quinoline to quinoline N-oxide (Table 1, entry 11), the present GNPs-RuO_2NPs catalyst is very effective (yielded 82 % after 4.5 h) compared to the $V_xSi_{4x}O_{6.4x}$ system which gave 71% of the desired product after 8 h.[15] It was found that the present catalytic system gave a moderate yield of 62% in the oxidation of quinoxaline to quinoxaline N-dioxide (Table 1, entry 12). A good yield of 91% was obtained from the oxidation of 2,2'-bipyridine after stirring for 4 h (Table 1, entry 13). The present catalytic system is less effective for the oxidation of sterically hindered heterocyclic amine. 2,2'-Biquinoline was oxidized to the corresponding N-dioxide in lower yield of 68% after stirring for 7 h (Table 1, entry 14). On contrary, in the oxidation of phenazine to the corresponding N-dioxide, the present catalytic system afforded a good yield of 86% (Table 1, entry 15). Alicyclic tertiary amine, quinuclidine, was oxidized to the corresponding amine oxide in an excellent yield of 94% (Table 1, entry 16). A good yield of 80% was obtained from the oxidation of 4-(dimethylamino)pyridine to the corresponding amine oxide after

Table 1 N-Oxidation of tertiary amines catalyzed by GNPs-RuO_2NPs[a]

Entry	Substrate	Product	Time (h)	Yield[b] (%)
1			4.0	98
2		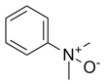	4.0	98
3	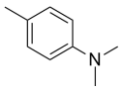	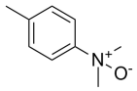	5.0	97
4[48]	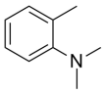	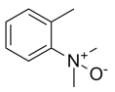	4.5	89
5[49]	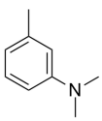	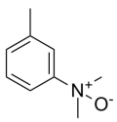	4.5	90
6	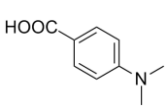	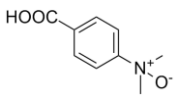	8.0	76
7	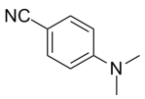	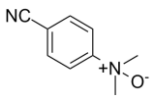	5.0	66
8[50]	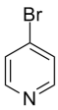	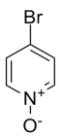	8.0	93
9			9.0	84
10	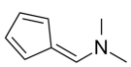	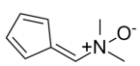	6.0	92
11		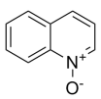	4.5	82
12[25]		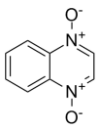	4.0	62
13[25]	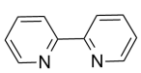	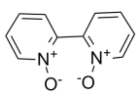	4.0	91

14	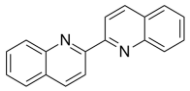	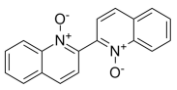	7.0	68
15[25]	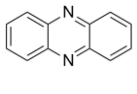	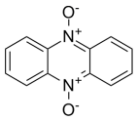	6.0	86
16			4.5	94
17[42]	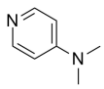	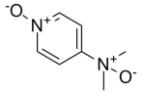	6.0	80
18	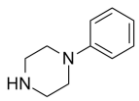	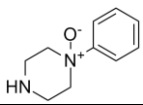	6.0	56

[a] Reaction conditions: Amine (2 mmol), GNPs-RuO_2NPs (0.13 mol%), H_2O_2 (5 mmol), acetonitrile (3 mL), 80 °C. [b] Isolated yield.

stirring for 6 h (Table 1, entry 17). Interestingly, the present catalytic system is highly selective towards the tertiary amine than the secondary one. In the oxidation of 1-phenylpiperazine (Table 1, entry 18), the catalytic system selectively oxidized the tertiary amine (56%). The excellent catalytic activity of the GNPs-RuO_2NPs with lower amount of Ru catalyst (0.13 mol%) is due to three most obvious reasons: (i) the smaller size of the RuO_2NPs, (ii) higher surface area of the GNPs-RuO_2NPs and (iii) an effective dispersion of the GNPs-RuO_2NPs in the reaction medium.

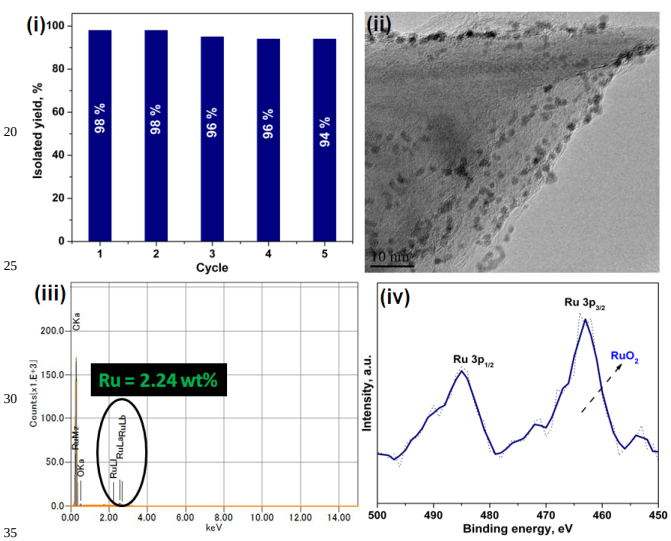

Fig. 8 (i) Reusability of GNPs-RuO_2NPs, (ii) TEM image, (iii) EDS and (iv) XPS of *u*-GNPs-RuO_2NPs.

Heterogeneity and reusability of GNPs-RuO_2NPs

To study the heterogeneity of the GNPs-RuO_2NPs, the nanocatalyst was separated out from the reaction mixture by a simple centrifugation and then the filtrate was analyzed by ICP-MS; no Ru content confirmed the heterogeneous nature of the GNPs-RuO_2NPs. Since the reusability of nanocatalyst is an important advantage, the separated GNPs-RuO_2NPs were washed with diethyl ether and dried in *vacuo* at 80°C. Then the recovered GNPs-RuO_2NPs were reused for the oxidation of triethylamine [Fig. 8(i)]. Interestingly, the present catalytic system afforded 94% of triethylamine N-oxide even at the 5th cycle, which confirmed its excellent reusability. Additionally, used nanocatalyst (*u*-GNPs-RuO_2NPs) was characterized by TEM, SEM-EDS and XPS analysis. The TEM image [Fig. 8(ii)] showed that the morphology of *u*-GNPs-RuO_2NPs remains unchanged. SEM-EDS result [Fig. 8(iii)] revealed that the weight percentage of Ru in *u*-GNPs-RuO_2NPs was 2.24. The chemical state of Ru in *u*-GNPs-RuO_2NPs was +4, as confirmed by XPS analysis [Fig. 8(iv)]. Therefore, GNPs-RuO_2NPs are physically as well as chemically stable and reusable.

Proposed mechanism

In order to understand the mechanism of GNPs-RuO_2NPs-catalyzed N-oxidation of tertiary amines, FT-IR (see Fig. S1 in ESI) and XPS spectra were recorded for pure GNPs-RuO_2NPs and *o*-GNPs-RuO_2NPs (the catalyst after stirring with H_2O_2 in CH_3CN at 80 °C for 4 h); results are shown in Fig. 9. In the FT-IR spectra, the peak at 1600 cm^{-1} was attributed to C=C stretching of GNPs.[30] Further, a new peak at 850 cm^{-1} was observed for *o*-GNPs-RuO_2NPs when compared to GNPs-RuO_2NPs, which proves the formation of Ru-oxo species.[44,45] Moreover, in comparison to pure GNPs-RuO_2NPs, O1s spectrum of *o*-GNPs-RuO_2NPs showed a dramatic increase in the peak intensity at 531.0 eV; this too clearly confirmed the formation of oxygen species on the RuO_2NPs during the N-oxidation reaction.[46] Kim *et al*.,[47] investigated the formation of various oxygen species on the RuO_2 surface under various conditions. They found that the oxygen species formed on the RuO_2 surface can play a very effective role in oxidation reactions. The results concluded that the mechanism for the N-oxidation of tertiary amines might be involving the oxygen species, possibly Ru-oxo species, as an

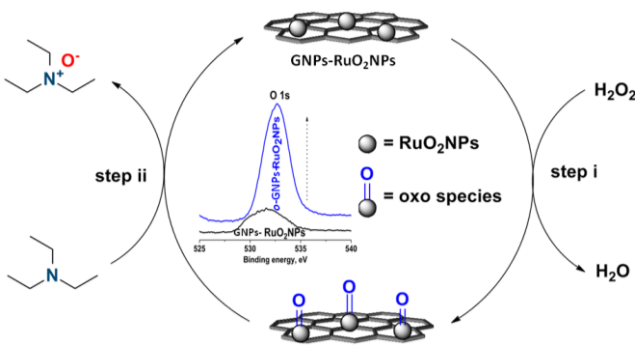

Fig. 9 Proposed catalytic mechanism for the N-oxidation of triethylamine using GNPs-RuO_2NPs.

intermediate (Fig. 9). In step (i), H_2O_2 helps for the formation Ru-oxo species by transferring its oxygen. Subsequently, in step (ii), the formed Ru-oxo species assists the formation of triethylamine N-oxide from triethylamine. Finally, GNPs-RuO_2NPs were regenerated for the further N-oxidation process.

Conclusions

RuO_2NPs with a mean diameter of 1.3 nm were decorated on *f*-GNPs by a straight forward "dry synthesis" method. TEM images showed an excellent attachment and homogeneous dispersion of RuO_2NPs on GNPs. The weight percentage of Ru in GNPs-RuO_2NPs was 2.68, as determined by EDS analysis. Raman intensity ratios confirmed the good attachment of RuO_2NPs on the surface of GNPs. XRD and XPS revealed that the Ru was in +4 oxidation state with a nano-crystalline nature of RuO_2NPs. The N-oxidation of tertiary amines could be carried out effectively with as low as 0.13 mol% of supported Ru catalyst for a wide range of substrates. To the best of our knowledge, this is the lowest amount of Ru used for the N-oxidation reaction. The proposed catalyst was chemically as well as physically very stable, heterogeneous in nature and could be reused up to 5 cycles. In summary, we have developed a heterogeneous Ru based nanocatalytic system for the N-oxidation of tertiary amines, which requires only a lower amount of catalyst (0.13 mol% of Ru) for efficient reaction.

Acknowledgements

This work was supported by the grant-in-aid for global COE program by the Ministry of Education, Culture, Sports, Science, and Technology, Japan. R.K. thanks DST (Govt. of India) for financial support under FIST programme.

Notes and references

[a]*Nano Fusion Technology Research Lab, Interdisciplinary Graduate School of Science and Technology, Shinshu University, Ueda, Nagano–386 8567, Japan. Fax: +81 268 21 5482, Tel: +81 268 21 5139, E–mail: weikai@shinshu–u.ac.jp*
[b]*SRM Research Institute, SRM University, Kattankulathur 603203, India*
[c]*College of Textile Clothing Engineering, Soochow University, Suzhou, 215021, China*
[d]*Department of Chemistry, National Institute of Technology, Tiruchirappalli–620 015, India. Fax: +91 431 2500133 Tel.: + 91 431 2503636, E–mail: kar@nitt.edu*

† Electronic Supplementary Information (ESI) available: ^{1}H-NMR and ^{13}C-NMR and FT-IR spectra. See DOI: 10.1039/b000000x/

1 K. Othmer, Encyclopedia of Chemical Technology, Eds: J. J. Mcketta, W. A. Cunningham, Wiley-VCH, New York, 1997, 33, 1.
2 J. H. Boyer, *Chem. Rev*., 1980, **80**, 495.
3 L. C. Campeau, D. R. Stuart, J. P. Leclerc, M. B. Laperle, E. Villemure, H. Y. Sun, S. Lasserre, N. Guimond, M. Lecavallier, K. Fagnou, *J. Am. Chem. Soc*., 2009, **131**, 3291.
4 V. Vanrheenen, D. Y. Cha, W. M. Hartley, *Org. Synth*. 1988, **6**, 342.
5 K. I. Priyadarsini, M. F. Dennis, M. A. Naylor, M. R. L. Stratford, P. Wardman, *J. Am. Chem. Soc*., 1996, **118**, 5648.
6 A. V. Malkov, M. Bell, F. Castelluzzo, P. Kocovsky, *Org. Lett*. 2005, **7**, 3219.
7 M. Schroder, *Chem. Rev*., 1980, **80**, 187.
8 A. V. Malkov, P. Kocovsky, *Eur. J. Org. Chem*., 2007, 29.
9 A. L. Baumstark, M. Dotrong, P. C. Vasquez, *Tetrahedron Lett*., 1987, **28**, 1963.
10 G. B. Payne, P. H. Deming, P. H. Williams, *J. Org. Chem*., 1961, **26**, 659.
11 J. G. Robhe, E. J. Behrman, *J. Chem. Res*. S 1993, 412.
12 M. Ferrer, F. Sanchez-Baeza, A. Messgure, *Tetrahedron* 1997, **53**, 15877.
13 H. S. Mosher, L. Turner, A. Carlsmith, *Org. Synth*., 1963, **4**, 828.
14 P. Brougham, M. S. Cooper, D. A. Cummerson, H. Heaney, N. Thomson, *Synthesis* 1987, 1015.
15 L. Rout, T. Punniyamurthy, *Adv. Synth. Catal*., 2005, **347**, 1958.
16 C. Coperet, H. Adolfsson, T. A. V. Khuong, A. K. Yudin, K. B. Sharpless, *J. Org. Chem*., 1998, **63**, 1740.
17 M. R. Prasad, G. Kamalakar, G. Madhavi, S. J. Kulkarni and K. V. Raghavan, *Chem. Commun*., 2000, 1577.
18 A. J. Bailey, W. P. Griffith, B. C. Parkin, *J. Chem. Soc. Dalton Trans*. 1995, 1833.
19 B. M. Choudary, B. Bharathi, Ch. Venkat Reddy, M. Lakshmi Kantam, *Green Chem*., 2002, **4**, 279.
20 P. Phukan, R.S. Khisti, A. Sudalai, *J. Mol. Catal. A: Chem*., 2006, **248**, 109.
21 D. J. Robinson, P. McMorn, D. Bethell, P. C. Bulman-Page, C. Sly, F. King, F. E. Hancock, G. J. Hutchings, *Catal. Lett*., 2001, **72**, 233.
22 M. Comotti, C. Della Pina, M. Rossi, *J. Mol. Catal. A: Chem*., 2006, **251**, 89.
23 C. Della Pina, E. Falletta, M. Rossi, *Top. Catal*., 2007, **44**, 325.
24 M. Pagliaro, S. Campestrini, R. Ciriminna, *Chem. Soc. Rev*., 2005, **34**, 837.
25 P. Veerakumar, S. Balakumar, M. Velayudham, K. L. Luc, S. Rajagopal, *Catal. Sci. Technol*., 2012, **2**, 1140.
26 X. Yanga, X. Wanga, J. Qiua, *Appl. Catal. A: Gen*., 2010, **382**, 131.
27 S. H. Joo, J. Y. Park, J. R. Renzas, D. R. Butcher, W. Y. Huang, G. A. Somorjai, *Nano Lett*., 2010, **10**, 2709.
28 A. Mondal, A. Sinha, A. Saha, N. R. Jana, *Chem. Asian J*., 2012, **7**, 2931.
29 A. V. Krasheninnikov, P. O. Lehtinen, A. S. Foster, P. Pyykko, R. M. Nieminen, *Phys. Rev. Lett*., 2009, **102**, 126807.
30 M. Gopiraman, S. G. Babu, K. Zeeshan, W. Kai, Y. A. Kim, M. Endo, R. Karvembu, I. S. Kim, *J. Phys. Chem. C* 2013, **117**, 23582.
31 M. Gopiraman, S. G. Babu, Z. Khatri, K. Wei, M. Endo, R. Karvembu, I. S. Kim, *Catal. Sci. Technol*., 2013, **3**, 1485.
32 Y. Lin, K. A. Watson, M. J. Fallbach, S. Ghose, J. G. Smith, D. M. Delozier, W. Cao, R. E. Crooks, J. W. Connell, ACS Nano 2009, **3**, 871.
33 O. Akhavan, *Carbon* 2010, **48**, 509.
34 V. Datsyuk, M. Kalyva, K. Papagelis, J. Parthenios, D. Tasis, A. Siokou, I. Kallitsis, C. Galiotis, *Carbon* 2008, **46**, 833.
35 G. Gil, P. A. A. P. Marques, C. M. Granadeiro, H. I. S. Nogueira, M. K. Singh, J. Gracio, *Chem. Mater*., 2009, **21**, 4796.
36 S. Shrestha, W. C. Choi, W. Song, Y. T. Kwon, S. P. Shrestha, C. Y. Park, *Carbon* 2010, **48**, 54.
37 J. Sankar, T. K. Sham, R. J. Puddephatt, *J. Mater. Chem*., 1999, **9**, 2439.
38 X. Zhou, X. Huang, X. Qi, S. Wu, C. Xue, F. Y. C. Boey, Q. Yan, P. Chen, H. Zhang, *J. Phys. Chem. C* 2009, **113**, 10842.
39 O. Akhavan, *ACS Nano* 2010, **4**, 4174.
40 M. Gopiraman, S. G. Babu, Z. Khatri, W. Kai, Y. A. Kim, M. Endo, R.

Karvembu, I. S. Kim, *Carbon* 2013, **62**, 135.
41 M. R. Prasad, G. Kamalakar, G. Madhavi, S. J. Kulkarni, K. V. Raghavan, *J. Mol. Catal. A: Chem.*, 2002, **186**, 109.
42 C. Marco, S. Alessandro, S. Giorgio, *Green Chem*. 2008, **10**, 793–798.
43 F. F. Bamoharrama, M. M. Heravi, M. Roshani, N. Tavakoli, *J. Mol. Catal. A: Chem.*, 2006, **252**, 219.
44 H. Saburo, N. Satoshi, T. Makoto, U. Kazunori, K. Hiroyoshi, I. Seiichiro, *Appl. Catal. A: Gen*., 2005, **288**, 67.
45 M. C. Chi, F. L. Ting, Y. W. Kwok, *Inorg. Chem*., 1987, **26**, 2289.
46 Y. Hirai, T. Kojima, Y. Mizutani, Y. Shiota, K. Yoshizawa, S. Fukuzumi, *Angew. Chem. Int. Ed*., 2008, **47**, 5772.
47 Y. D. Kim, A. P. Seitsonen, S. Wendt, J. Wang, C. Fan, K. Jacobi, H. Over, G. Ertl, *J. Phys. Chem. B* 2001, **105**, 3752.
48 C. F. Xue; Z. Hui, L. Xiaohua, Q. Bo, F. Xiaoming, Z. Guolin, J. Yaozhong, *Chem. Eur. J*., 2004, **10**, 4790.
49 A. K. T. Al-Allaf, A. M. T. Al-Tayy, *J. Organomet. Chem.*, 1990, **391**, 37.
50 K. Laihia, *J. Mol. Struct.*, 2006, **783**, 73.

